
Towards Fundamentally Scalable Model Selection: Asymptotically Fast Update and Selection

Wenxiao Wang*
University of Maryland
wwx@umd.edu

Weiming Zhuang
Sony AI
weiming.zhuang@sony.com

Lingjuan Lyu†
Sony AI
lingjuan.lv@sony.com

Abstract

The advancement of deep learning technologies is bringing new models every day, motivating the study of scalable model selection. An ideal model selection scheme should minimally support two operations efficiently over a large pool of candidate models: **update**, which involves either adding a new candidate model or removing an existing candidate model, and **selection**, which involves locating highly performing models for a given task. However, previous solutions to model selection require high computational complexity for at least one of these two operations. In this work, we target fundamentally (more) scalable model selection that supports asymptotically fast update and asymptotically fast selection at the same time. **Firstly**, we define **isolated model embedding**, a family of model selection schemes supporting asymptotically fast update and selection: With respect to the number of candidate models m , the update complexity is $O(1)$ and the selection consists of a single sweep over m vectors in addition to $O(1)$ model operations. Isolated model embedding also implies several desirable properties for applications. **Secondly**, we present **Standardized Embedder**, an empirical realization of isolated model embedding. We assess its effectiveness by using it to select representations from a pool of 100 pre-trained vision models for classification tasks and measuring the performance gaps between the selected models and the best candidates with a linear probing protocol. Experiments suggest our realization is effective in selecting models with competitive performances and highlight isolated model embedding as a promising direction towards model selection that is fundamentally (more) scalable.

1 Introduction

New models are being created and becoming available at a rate beyond previous imaginations. Hugging Face Hub, a web platform for hosting machine learning models, datasets, and demo applications, included more than 300k pre-trained models in August 2023, when its owner, the company named Hugging Face, obtained a \$4.5 billion valuation while raising funding of \$235 million backed by multiple investors.³ Such vast amounts of models will become more valuable if we can identify the ones suitable for tasks of interest, motivating the study of scalable model selection.

Arguably, an ideal model selection scheme should minimally be able to support two operations efficiently over a large number of candidate models, which are update and selection. **Update** is an operation to either add a new candidate model or to remove an existing candidate model, which is necessary for keeping a dynamic model pool that is up-to-date. **Selection** is an operation to locate

*Work done during Wenxiao’s internship at Sony AI.

†Corresponding Author.

³[https://www.nasdaq.com/articles/ai-startup-hugging-face-valued-at-\\$4.5-bl-in-latest-round-of-funding](https://www.nasdaq.com/articles/ai-startup-hugging-face-valued-at-$4.5-bl-in-latest-round-of-funding)

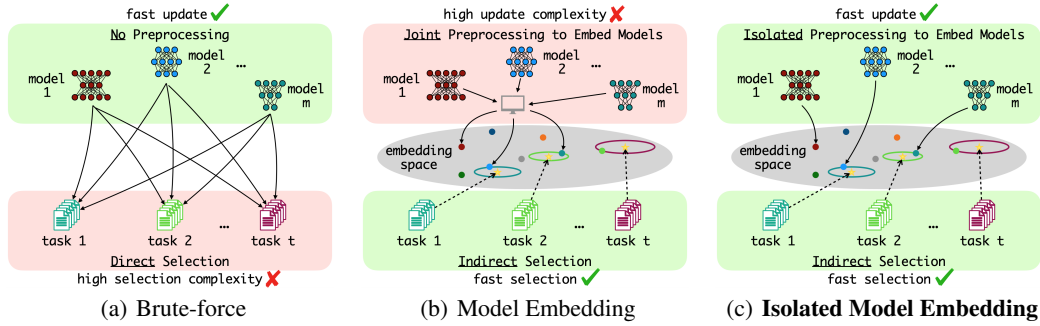


Figure 1: Illustrations for different families of model selection schemes. **Isolated model embedding (ours)** is a family that supports asymptotically fast update and selection **at the same time**.

proper models for a given task, which is the core functionality of model selection. Unfortunately, existing solutions require high computational complexity for at least one of these two operations.

The most naive solution for model selection is to directly examine every candidate model on the given task for each selection operation, i.e. a brute-force solution as illustrated in Figure 1(a). Consequently, the computational complexity, measured by the number of model operations (e.g. forward/backward passes), is linear to the number of candidate models for **each selection operation**. Such complexity is prohibitively high when dealing with a large number of models and with multiple downstream tasks (i.e. multiple selection operations), even when using transferability metrics [3, 33, 51, 34, 23, 2, 4] as surrogates to reduce the computational cost of model training/tuning.

Model embedding offers a direction to improve selection complexity. Rising from the study of task similarities [55, 1, 27, 56], Model2Vec [1] computes an embedding vector for each candidate model, which can be used repeatedly across multiple selection operations. For each selection operation, a task embedding will first be computed using the corresponding downstream data, which takes a bounded amount of model operations that is independent from the number of candidate models, and then be used to compare with pre-computed model embeddings to locate the promising candidate models, which takes a single sweep over the model embeddings. As a result, with respect to the number of candidate models m , the number of model operations per selection is reduced to $O(1)$ with the cost of a single additional sweep over m vectors. An illustration is provided in Figure 1(b).

However, Model2Vec computes the model embeddings through a joint optimization that involves all candidate models, meaning that the Model2Vec embedding of each model depends on not only the model itself but also other ones in the candidate pool. This implies high complexity for each update operation that is linear to the number of candidate models (assuming no major algorithmic change) as existing model embeddings are subject to change with the addition of any new candidate model.

In this work, we target fundamentally (more) scalable model selection that supports asymptotically fast update and asymptotically fast selection at the same time. Specifically:

(1) We define **isolated model embedding**, a family of model selection schemes with asymptotically fast update and selection. Intuitively, isolated model embedding refers to a subset of the model embedding family where computing the embedding of each individual model is isolated from the others, as illustrated in Figure 1(c). In another word, the embedding of each model will be independent from other models in the candidate pool, which implies that each update operation involves only a single candidate model as all the previously computed model embeddings stay unchanged. Thus for isolated model embedding, with respect to the number of candidate models m , the update complexity is $O(1)$ and the selection consists of a single sweep over m vectors in addition to $O(1)$ model operations. Notably, isolated model embedding also implies several other desirable properties.

(2) We present **Standardized Embedder**, an empirical realization of isolated model embedding. The key intuition of Standardized Embedder is standardization, i.e. using one public model as the baseline to embed all different candidate models, thus ensuring the independently learned embedding vectors conform to the same standard and are therefore comparable. We use it to select representations from a pool of 100 pre-trained vision models for classification tasks and assess the performance gaps between the selected models and the best candidates with a linear probing protocol. Experiments

suggest our realization is effective in selecting competitive models and highlight isolated model embedding as a promising direction towards fundamentally (more) scalable model selection.

2 Related Work

Transferability metrics for model selection. Intuitively, transferability metrics are scores that correlate with the performance of models/features after being transferred to a new task and can be computed without training: H-score [3] is defined by incorporating the estimated inter-class variance and the redundancy of features; LEEP [33] estimates the distribution of target task label conditioned on the label of pre-trained tasks to construct a downstream classifier without training and use its performance as the metric; LogME [51] estimates the maximum value of the marginalized likelihood of the label given pre-trained features and uses its logarithm as the score; GBC [34] uses class-wise Gaussians to approximate downstream samples in the pre-trained feature space so that class overlaps can be computed with Bhattacharyya coefficients to serve as a score; TransRate [23] estimates mutual information between features and labels by resorting to coding rate. Separate evaluations of transferability metrics are conducted by Agostinelli et al. [2] and Bolya et al. [4].

Model embedding for model selection. Model2Vec is proposed jointly with Task2Vec by Achille et al. [1]. The goal of Task2Vec is to embed different tasks into a shared vector space and it does so by estimating the Fisher information matrix with respect to a probe network. To embed models, they first initialize the embedding of each model as the sum of the Task2Vec embedding F of its pre-trained task (which is set to 0 if the task is unknown) and a learnable perturbation b . Then they learn the perturbations of all models jointly by predicting the best model given the distances of model embeddings to the task embeddings, which requires access to multiple downstream tasks in advance.

3 A Family of Model Selection with Asymptotically Fast Update and Selection

3.1 Formal Definition

Isolated model embedding, as we defined, is a family of model selection schemes consisting of two parts, as illustrated in Figure 1(c): (1) **preprocessing**, where candidate models are converted into embedding vectors for later use in selecting models; (2) **selection**, where models are selected given downstream data (i.e. data corresponding to the downstream task) and the model embeddings generated during preprocessing.

Preprocessing. The preprocessing part is defined by a model embedding function of the form $\mathcal{P}(\text{model}) \rightarrow \mathcal{V}$, where ‘model’ denotes a single (candidate) model and \mathcal{V} denotes an embedding space. Intuitively, \mathcal{P} maps a single model into its corresponding embedding vectors. Let f_1, f_2, \dots, f_m be all current candidate models where m is the total number of candidate models. For preprocessing, embedding vectors of all candidate models are generated as $\{v_i = \mathcal{P}(f_i)\}_{i=1}^m$, where v_i is the embedding vector corresponding to the candidate model f_i . Notably, this definition naturally enforces the model embedding process to be isolated: The model embedding function \mathcal{P} takes a single candidate model as its input and is applied independently to each candidate model, which means the computing of each individual embedding is isolated from other models in the candidate pool. *Update operations* of isolated model embedding are defined within preprocessing, where adding a new model is essentially computing its corresponding embeddings with the model embedding function \mathcal{P} and removing a candidate model is removing its corresponding model embedding.

Selection. The selection part is defined by a task embedding function of the form $\mathcal{Q}(\text{data}) \rightarrow \mathcal{V}$ and a selection metric of the form $\delta : \mathcal{V} \times \mathcal{V} \rightarrow \mathbb{R}$, where ‘data’ denotes the downstream data and \mathcal{V} denotes again the embedding space. These define the **selection operations** of isolated model embedding. For each selection operation, a task embedding vector v_{task} will first be computed by applying the task embedding function \mathcal{Q} to the downstream data and then be compared with pre-computed model embeddings to locate promising candidate models by finding model embeddings v_i that maximize the selection metric $\delta(v_{\text{task}}, v_i)$.

Table 1: A summary of the computational complexity per operation for different families of model selection schemes with respect to the (current) number of candidate models m . *Selection complexity is measured by the number of model operations, e.g. forward/backward passes of models.

Family	Update Complexity	Selection Complexity*
Brute-force	$O(1)$	$O(m)$
Model embedding	$O(m)$	$O(1)$
Isolated model embedding	$O(1)$	$O(1)$

3.2 Asymptotically Fast Update and Selection

In this section, we show how isolated model embedding supports asymptotically fast update and selection by analyzing computational complexity. A summary of update complexity and selection complexity for different families of model selection schemes is included in Table 1.

Update complexity: An update operation either adds a new candidate model or removes an existing one. With isolated model embedding, adding a new model is essentially computing its corresponding embeddings with the model embedding function \mathcal{P} . Since the model embedding function \mathcal{P} takes a single model as its input and has no dependency on the number of the candidate models m , the computational complexity of \mathcal{P} (and therefore the complexity of adding a new model) must be $O(1)$ with respect to m . Removing a candidate model is simply removing its corresponding embedding vectors from a maintained list containing embeddings of all the (current) candidate models, which can also be $O(1)$. Thus with respect to the number of candidate models m , the complexity per update operation is $O(1)$ for isolated model embedding.

Selection complexity: With isolated model embedding, a selection operation consists of two steps. The first step is to use the task embedding function \mathcal{Q} to compute a task embedding vector v_{task} . The task embedding function \mathcal{Q} takes the downstream task data as the input and has no dependency on the number of the candidate models m , thus the computational complexity of \mathcal{Q} is $O(1)$ with respect to m , which also means that there can be at most $O(1)$ model operations. The second step is to compare the task embedding v_{task} with the model embeddings $\{v_i\}_{i=1}^m$ by computing the selection metric $\delta(v_{\text{task}}, v_i)$, which takes a single sweep over m model embedding vectors. As a result, with respect to the number of candidate models m , each selection operation consists of $O(1)$ model operations in addition to a single sweep over m embedding vectors. Notably, while the selection complexity is technically still $O(m)$, reducing the number of model operations from $O(m)$ to $O(1)$ greatly improves scalability, as model operations (e.g. forward/backward passes) are typically orders of magnitude slower than vector operations (e.g. inner products) in practice.

3.3 Other Desirable Properties

Isolated model embedding is naturally decentralizable. Model owners can make their models candidates of future model selections entirely on their own, requiring no collaboration with other model owners and requiring no centralized coordination. Given the model embedding function \mathcal{P} , model owners can independently embed their models and publish/broadcast the resulting embeddings by themselves. After that, any party can use the task embedding function \mathcal{Q} and the selection metric δ to select models for its own tasks, using all the model embeddings that it has access to. This is a quite simple decentralized protocol from isolated model embedding.

Embedding vectors are flexible and portable information carriers. Model embeddings are simply (real) vectors, which can be stored and processed in diverse formats through various packages, making it a bridge connecting different implementation frameworks, different owners and different platforms. For example, some model owners may use PyTorch for their models and for implementing the model embedding function \mathcal{P} while some model owners may use TensorFlow, but this creates little difficulty for a selection operation even if it is implemented in neither frameworks since the selection operation only needs to recognize the computed embedding vectors. In addition, typical dimensions of model embeddings are fairly small and therefore the sizes are quite portable: For instance, in later empirical evaluations, we incorporate settings with 512-dimensional and 768-dimensional model embeddings, while as an informal comparison, each of Figure 1(a), 1(b) and 1(c) contains $1372 \times 1190 \approx 1.6 \times 10^6$

RGB pixels, which is about 4.8×10^6 dimensions with 8 bits each. Thus a single image of such has already enough bits to encode the embedding vectors as 32-bit floats for more than 1000 models.

Candidate models can be kept private throughout model selection. Model owners can embed their models using the model embedding function \mathcal{P} by themselves, and the only model-dependent information required by selection operations is the model embeddings. Thus, for the entire model selection process, model owners do not need to release their models to any other parties, including but not limited to other model owners and downstream users who want to select models for their downstream tasks. As selection completes, downstream users can reach out to the owners of selected candidates (instead of all model owners) for requesting access.

Selection operations can be made invisible to model owners. Given the model embeddings, selection operations can be performed fully locally by downstream users. Consequently, downstream data can be kept private and model owners will have no knowledge regarding the selection or whether there is a selection, unless the downstream users choose to notify them. This can be a highly valuable privacy guarantee for downstream users.

4 Standardized Embedder: A Realization of Isolated Model Embedding

In this section, we present Standardized Embedder, an empirical realization of isolated model embedding. As defined in Section 3 and illustrated in Figure 1(c), isolated model embedding contains two parts: **preprocessing**, where model embedding vectors are learned independently for different candidates, and **selection**, where a task embedding vector is learned from the downstream data and is used to search among model embeddings to guide model selection. We will introduce some concepts as tools in Section 4.1 before we present these two parts respectively in Section 4.2 and 4.3.

4.1 Tool: (Approximate) Functionality Equivalence

Firstly, we introduce notations. Let \mathcal{X} be the input space. A feature $f : \mathcal{X} \rightarrow \mathbb{R}$ is defined as a function mapping any sample from the input space \mathcal{X} to a real number. A set of features F is therefore a set of functions, which can also be considered as a function $F : \mathcal{X} \rightarrow \mathbb{R}^n$ mapping any sample to a vector of n dimensions, where n can be either finite or countably infinite, depending on whether or not the set contains a finite number of features.

Definition 4.1 (Functionality Equivalence). For two sets $F : \mathcal{X} \rightarrow \mathbb{R}^n$ and $\hat{F} : \mathcal{X} \rightarrow \mathbb{R}^m$ of features, they are considered δ -equivalent in functionality over a distribution D over \mathcal{X} , if and only if there exist two affine transformations $w, b \in \mathbb{R}^{n \times m} \times \mathbb{R}^m$ and $\hat{w}, \hat{b} \in \mathbb{R}^{m \times n} \times \mathbb{R}^n$ such that

$$\mathbb{E}_{x \sim D} \left[S_{\cos} \left(w^\top F(x) + b, \hat{F}(x) \right) \right] \geq 1 - \delta \quad \text{and} \quad \mathbb{E}_{x \sim D} \left[S_{\cos} \left(F(x), \hat{w}^\top \hat{F}(x) + \hat{b} \right) \right] \geq 1 - \delta,$$

where $S_{\cos}(u, v)$ denotes cosine similarity between two vectors u and v .

Functionality equivalence characterizes cases where two sets of features are considered the same regarding their usability in unknown applications. Intuitively, since most (if not all) modern architectures of neural networks have at least one affine transformation following the feature layers, two sets of features should be considered equivalent even if they differ by an affine transformation. Similar arguments are introduced by [48] to understand deep representations, where they consider two representations to be equivalent when the subspaces spanned by their activation vectors are identical. While in principle other similarity metrics can be utilized as well, we use cosine similarity in this work since it is naturally invariant to feature scalings.

4.2 Preprocessing: Isolated Model Embedding by Identifying Equivalent Feature Subsets

With functionality equivalence from Definition 4.1, we can characterize the representation powers of any set of features by associating them with the equivalent subsets from a pre-defined, baseline feature set $B : \mathcal{X} \rightarrow \mathbb{R}^N$ (Empirically we will use a public model as this baseline feature set, which will be elaborated in Section 5). Since any subset of the baseline feature set $B : \mathcal{X} \rightarrow \mathbb{R}^N$ can be directly associated with a binary vector from $\{0, 1\}^N$ (i.e. each 1 indicating the presence of a feature and each 0 indicating an absence; See Appendix C for examples), we simply use such vectors as the embeddings of models. For the actual implementation, we relax this binary embedding space to a continuous one (i.e. $[0, 1]^N$). The formal definition is as follows.

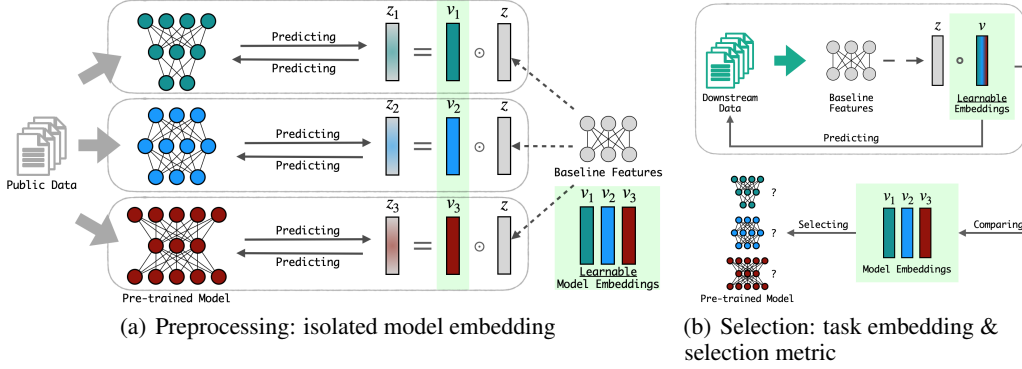


Figure 2: An illustration of Standardized Embedder. **(a) Preprocessing:** Using features of a public model as the baseline, a vector embedding is learned **independently** for each pre-trained model. Intuitively, the embeddings of models denote their approximately equivalent feature subsets in the baseline features. **(b) Selection:** Task embeddings are defined by subsets of the baseline features that are important to corresponding downstream tasks, which are identified through enforcing sparsity regularization. Models are selected by comparing the task embedding with model embeddings of all candidates, using (the cardinality of) standard fuzzy set intersection as the selection metric.

Definition 4.2 (Vector Embedding through Equivalent Feature Subsets). Given a baseline feature set $B : \mathcal{X} \rightarrow \mathbb{R}^N$, a vector $v \in \{0, 1\}^N$ is a δ -embedding vector of a feature set $F : \mathcal{X} \rightarrow \mathbb{R}^n$ over a distribution D if and only if F and $\{B_i | v_i = 1\}$ are δ -equivalent in functionality over D .

Given a set of features as the baseline, the embedding vectors corresponding to a set of features are defined through Definition 4.2. Consequently, we can now conceptually map each model, represented as a set of features, into a vector embedding space that associates with the baseline features.

In practice, to compute the embedding vectors given baseline features, we relax the binary embedding space to a continuous one and reformulate it as follows:

$$\begin{aligned} & \max_{v, w, b, \hat{w}, \hat{b}} \min (L_{\text{to baseline}}, L_{\text{from baseline}}) \\ \text{subject to: } & L_{\text{to baseline}} = \mathbb{E}_{x \sim D} [S_{\cos}(w^\top F(x) + b, v \odot B(x))] \\ & L_{\text{from baseline}} = \mathbb{E}_{x \sim D} [S_{\cos}(F(x), \hat{w}^\top (v \odot B(x)) + \hat{b})] \\ & v \in [0, 1]^n, w \in \mathbb{R}^{n \times N}, b \in \mathbb{R}^N, \hat{w} \in \mathbb{R}^{N \times n}, \hat{b} \in \mathbb{R}^n \end{aligned}$$

where $F : \mathcal{X} \rightarrow \mathbb{R}^n$ is the feature set that we want to vectorize, $B : \mathcal{X} \rightarrow \mathbb{R}^N$ is the set of baseline features, D is the underlying data distribution, v is the (relaxed) embedding vector, w, b, \hat{w}, \hat{b} are parameters of affine transforms and \odot denotes Hadamard product (i.e. element-wise multiplication). An illustration of the model embedding process is included in Figure 2(a).

Empirically, the constraint $v \in [0, 1]^n$ is implemented via reparameterization through the sigmoid function, i.e. $v_i = 1/(1 + e^{-v_i'/\tau})$, where τ is a constant known as temperature and we use a fixed temperature of $\tau = 0.01$ in all experiments. Intuitively, the optimization wants to find a subset of the baseline features (indicated by the mask v) that is δ -equivalent to F for smaller δ .

Both Definition 4.2 and the relaxation are straightforward, but it is worth noting that the embedding depends on not only the model (i.e. the set of features) to be embedded, but also the set of baseline features, and the embedding vectors may not be unique by definition depending on the choice of baseline features. Conceptually, what we do here is to compare the embedding distributions of different models by drawing a single embedding vector from each distribution.

4.3 Selection: Task Embedding through Feature Sifting

In this section, we showcase how to derive a task embedding vector from downstream data and the selection metric for comparing the task embedding with model embeddings. An illustration of the

process is included in Figure 2(b): Intuitively, we derive the task embedding vector by identifying subsets of the baseline features $B : \mathcal{X} \rightarrow \mathbb{R}^N$ that are important to the task of interest, which can then be directly associated with binary vectors from $\{0, 1\}^N$, similar to how we previously embed models as vectors, and we use a measure of (fuzzy) set similarity as the selection metric.

Formally, for a downstream task, let \mathcal{X} be the input space, \mathcal{Y} be the label space, we use \hat{D} to denote the downstream data distribution, which is a distribution over $\mathcal{X} \times \mathcal{Y}$. Using L to denote the corresponding task loss, identifying important features can be formulated as follows:

$$\min_{v, w, b} \mathbb{E}_{x, y \sim \hat{D}} [L(w^\top (v \odot B(x)) + b, y)] + \gamma \|v\|_1 \quad \text{subject to: } \|w^\top\|_1 = 1 \text{ and } v \in [0, 1]^n$$

where $v \in [0, 1]^n$ is the embedding vector of the task to be learned, $w, b \in \mathbb{R}^{n \times |\mathcal{Y}|} \times \mathbb{R}^{|\mathcal{Y}|}$ jointly denotes a prediction head associated with the task of interest, $\|v\|_1$ denotes the ℓ_1 norm of the embedding vector (which functions as sparsity regularization), $\|w^\top\|_1$ denotes the matrix norm of w^\top induced by ℓ_1 norm of vectors (i.e. $\|w^\top\|_1 = \sup_{x \neq 0} \|w^\top x\|_1 / \|x\|_1 = \max_i \sum_j |w_{ij}|$) and γ is sparsity level, a scalar hyper-parameter controlling the strength of the sparsity regularization $\gamma \|v\|_1$. A rule of thumb for choosing γ is suggested in Section 5.4.

Selection metric. Given the task embedding, we compare it with embeddings of candidate models to identify the most similar ones to the task embedding with respect to a similarity metric—the corresponding models are the ones to be selected. Notably, all our embedding vectors, including model embeddings and task embeddings, are relaxations of binary vectors denoting subsets of the baseline features. This is well related to fuzzy set theory [53, 24] where each element can have a degree of membership between 0 and 1 to indicate whether it is not/fully/partially included in a set. Interpreting both model embeddings and task embeddings as fuzzy sets, we incorporate standard fuzzy set intersection to measure the similarity between model embeddings and task embeddings. Formally, let $u, v \in [0, 1]^n$ be two embedding vectors (interpreted as fuzzy sets), the cardinality of their standard intersection is simply $I_{\text{standard}}(u, v) = \sum_{i=1}^n \min(u_i, v_i)$.

Intuitively, the task embedding denotes the set of baseline features useful for the task of interest and each model embedding denotes the set of baseline features possessed by the corresponding candidate model. Thus the cardinality of their intersection measures the quantity of the useful features owned by candidate models and therefore provides guidance for downstream performance.

5 Evaluation

5.1 Evaluation Setup

For evaluations, we gather **100 pre-trained models** with various architectures and training recipes as candidates of model selection. See Appendix A for the full list of models.

Preprocessing. Recalling that Standardized Embedder uses a public model as the baseline features and (approximate) functionality equivalence is defined over an underlying distribution D , we include two choices of baseline features, a pre-trained ResNet-18 or a pre-trained Swin Transformer (tiny) and we use the validation set of ImageNet (50000 samples in total) as the underlying distribution D (for the embedding of candidate models). We use the same hyper-parameters when embedding different candidate models: We use SGD optimizer with a batch size of 128, an initial learning rate of 0.1, a momentum of 0.9, and a weight decay of $5e-4$; We divide the learning rate by a factor of 10 every 1k steps for settings with 4k training steps (=10.24 epochs) per candidate, and every 3k steps for settings with 10k training steps (=25.6 epochs) per candidate.

Selection. We assess the quality of representations selected for three downstream benchmarks, CIFAR-10 [25], CIFAR-100 [25] and STL-10 [12], which are natural object classifications benchmarks with varying granularity and varying domain shifts (compared to ImageNet validation set that we use as the distribution to embed models). To learn task embeddings, we use SGD optimizer with a batch size of 128, an initial learning rate of 0.1, a momentum of 0.9, and a weight decay of $5e-4$ for 60 epochs, with the learning rate getting divided by a factor of 10 every 15 epochs. Notably, the weight decay is disabled for the task embedding to be learned to avoid interfering with the sparsity regularization from Section 4.3. For coherence, we discuss the choice of the sparsity level γ in Section 5.4.

Evaluation. To estimate performance gaps between the selected models and the best candidates, we incorporate a linear probing protocol commonly used to assess the quality of representations

Table 2: Empirical evaluations of Standardized Embedder with **100 pre-trained models** as the candidates (See Appendix A for the full list). Standardized Embedder successfully locates models comparable to the best candidates for corresponding downstream tasks.

Downstream task	Best candidate (Ground truth)	Model used as baseline features	Training steps per candidate	Downstream accuracy of selected models (+gap from the best candidate)		
				best of top 1	best of top 3	best of top 5
CIFAR-10	95.15%	ResNet-18	4k	91.81% (3.34%)	94.57% (0.58%)	94.57% (0.58%)
			10k	94.36% (0.79%)	95.12% (0.03%)	95.12% (0.03%)
		Swin-T (tiny)	4k	94.57% (0.58%)	94.57% (0.58%)	95.12% (0.03%)
			10k	95.12% (0.03%)	95.12% (0.03%)	95.12% (0.03%)
CIFAR-100	82.58%	ResNet-18	4k	81.11% (1.47%)	81.11% (1.47%)	81.11% (1.47%)
			10k	80.13% (2.45%)	80.13% (2.45%)	81.57% (1.01%)
		Swin-T (tiny)	4k	81.11% (1.47%)	81.48% (1.10%)	81.48% (1.10%)
			10k	81.48% (1.10%)	81.48% (1.10%)	81.48% (1.10%)
STL-10	99.24%	ResNet-18	4k	98.76% (0.47%)	98.76% (0.47%)	98.76% (0.47%)
			10k	97.51% (1.72%)	98.60% (0.64%)	98.76% (0.47%)
		Swin-T (tiny)	4k	97.69% (1.55%)	98.60% (0.64%)	98.60% (0.64%)
			10k	98.60% (0.64%)	98.60% (0.64%)	98.60% (0.64%)

[8, 21, 49, 10]. For every candidate model and for every downstream task, a linear head is trained over its features to compute the corresponding downstream accuracy. We use SGD with a batch size of 128, an initial learning rate of 0.1, a momentum of 0.9, and a weight decay of $5e-4$ for 60 epochs, with the learning rate getting divided by a factor of 10 every 15 epochs.

5.2 The Performance of Standardized Embedder

In Table 2, we include the quantitative evaluations on the performance of Standardized Embedder. For each downstream task, we report in the left half of the table the downstream accuracy of the best candidates (i.e. the ground truth) for references and report in the right half of the table the downstream accuracy of models selected (i.e. the top-1/top-3/top-5 candidates according to the selection metric). Standardized Embedder successfully locates models/representations comparable to the best possible candidates with respect to different downstream tasks: When selecting only 1 model from the 100 candidates, the **worst** accuracy gap **across all evaluated settings** of Standardized Embedder (i.e. with different baseline features and training steps per candidate) and all downstream tasks evaluated is 3.34%, which is reduced to 2.45% when selecting 3 models and 1.47% when selecting 5 models; When using Swin Transformer (tiny) as baseline features and 10k embedding steps per candidate, the worst gap is only 1.10% even when selecting only 1 model.

In Figure 3(a) and 3(b), we present both the downstream accuracy and the cardinality of standard intersection (i.e. the selection metric) for different downstream tasks when using different baseline features. More results are included in Figure 4 and 5 in Appendix. We use the **dashed line** to highlight the downstream accuracy of the public model used as baseline features. An important observation here is that Standardized Embedder is able to locate much more competitive models when the public model used as baseline features is only suboptimal (i.e. the public model used as baseline features performs considerably worse on the downstream tasks compared to the best possible candidate).

5.3 On the Choice of Baseline Features

Table 2 suggests that Standardized Embedder performs better when using Swin Transformer (tiny) as baseline features compared to when using ResNet-18. To further understand this, we compare the selection metric of candidate models on each of the evaluated downstream tasks when using different baseline features in Figure 3(c), with more results included in Figure 6 and Figure 7 in Appendix, where in all cases there are clusters of green/orange points in the bottom right, which corresponds to Transformers and hybrid models (i.e. models with both convolution and attention)

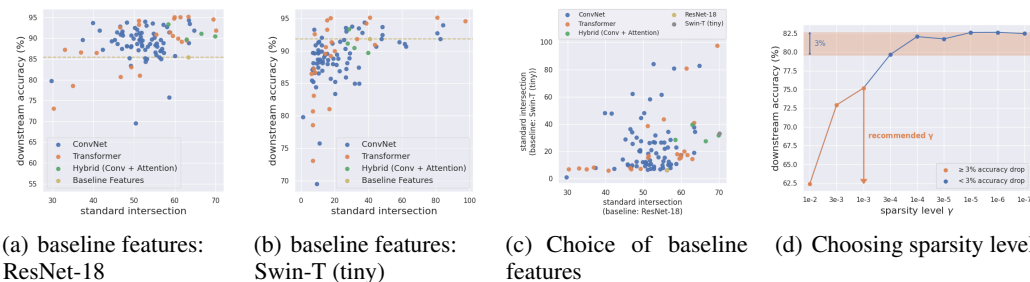


Figure 3: **(a, b)** Downstream accuracy (i.e. the ground truth) on CIFAR-10 v.s. the cardinality of standard intersections (i.e. the selection metric) when using 4k steps per candidate. The downstream accuracy of the baseline features are highlighted with the dashed line. When a public model is only suboptimal, using it as baseline features for Standardized Embedder can still locate more competitive models. See Figure 4 and 5 in Appendix for more results including other downstreams and more steps. **(c)** Comparing the cardinality of standard intersections (i.e. the selection metric) when using different baseline features (ResNet-18 and Swin-T (tiny)) with 4k steps per candidate and CIFAR-10 as the downstream task. The green/orange points in the bottom right suggest using ResNet-18 as baseline features tend to overestimate (some) models with attentions compared to using Swin Transformer (tiny). See Figure 6 and 7 in Appendix for more results including other downstreams and more steps. **(d)** Downstream accuracy on CIFAR-10 of the baseline features ResNet-18 corresponding to varying sparsity regularization γ . A rule of thumb for deciding the value of γ : using the smallest γ with at least 3% accuracy drop from the converged accuracy. See Figure 8 in Appendix for more results.

that are overrated when using ResNet-18 as baseline features. This is likely because the limited receptive fields of ConvNets prevents them from capturing some long-range correlations utilized by models with attention (i.e. Transformers and hybrid models), which suggests models with attention are currently better choices of baseline features than ConvNets.

A possible limitation of Standardized Embedder is the robustness of the choice of baseline features to primary paradigm shifts. While our results suggests that using ResNet-18, a ConvNet from 2015, remains effective with the presence of many models proposed after 2020 and/or based on attention, there is no theoretical guarantee regarding its robustness under major paradigm shifts in the future. If that is the case, the choice of baseline features might need to be updated accordingly upon new paradigms, which can obviously introduce additional computational overhead.

5.4 Choosing Sparsity Level in Task Embedding

In Section 4.3, we introduce a scalar hyper-parameter, the sparsity level γ , to control the strength of sparsity regularization $\gamma\|v\|_1$ when defining the embedding of the downstream task. Here we will present a rule of thumb that we use for choosing γ empirically in our experiments.

Intuitively, the sparsity regularization works by penalizing the use of any feature and therefore only features that are critical enough for the downstream task will be utilized. As the sparsity level γ increases, the subsets of features preserved will also be smaller. Informally, to determine the set of features necessary for the downstream task, one can keep increasing the sparsity level γ until the downstream performance starts to drop. In Figure 3(d), we include downstream accuracy of the baseline features corresponding to varying sparsity level γ to present a rule of thumb for deciding the values of sparsity level: simply using the smallest γ with at least 3% accuracy drop from the converged accuracy (i.e. the eventual accuracy when the sparsity level keeps decreasing). More results can be found in Figure 8 in Appendix. This single rule is applied to all experiments and it works well as previously presented in Section 5.2.

6 Conclusion

We define **isolated model embedding**, a family of model selection schemes where the update complexity is $O(1)$ and the selection consists of a single sweep over m vectors plus $O(1)$ model operations, both with respect to the number of candidate models m . Isolated model embedding also

implies several other desirable properties for applications. We present **Standardized Embedder**, an empirical realization of isolated model embedding. Our experiments with 100 vision models support its effectiveness and highlight isolated model embedding as a promising direction towards model selection that is fundamentally (more) scalable. While our experiments focus on visual classifications, the concept of isolated model embedding is modality- and task-agnostic. Thus a natural future direction will be to extend this approach to encompass a broader range of data types and tasks.

7 Acknowledgement

Wenxiao Wang would like to thank Samyadeep Basu from University of Maryland for relevant discussions prior to Wenxiao’s internship at Sony AI.

References

- [1] Alessandro Achille, Michael Lam, Rahul Tewari, Avinash Ravichandran, Subhansu Maji, Charles C. Fowlkes, Stefano Soatto, and Pietro Perona. Task2vec: Task embedding for meta-learning. In *Proceedings of the IEEE/CVF International Conference on Computer Vision (ICCV)*, October 2019.
- [2] Andrea Agostinelli, Michal Pándy, Jasper R. R. Uijlings, Thomas Mensink, and Vittorio Ferrari. How stable are transferability metrics evaluations? In Shai Avidan, Gabriel J. Brostow, Moustapha Cissé, Giovanni Maria Farinella, and Tal Hassner, editors, *Computer Vision - ECCV 2022 - 17th European Conference, Tel Aviv, Israel, October 23-27, 2022, Proceedings, Part XXXIV*, volume 13694 of *Lecture Notes in Computer Science*, pages 303–321. Springer, 2022. doi: 10.1007/978-3-031-19830-4_18. URL https://doi.org/10.1007/978-3-031-19830-4_18.
- [3] Yajie Bao, Yang Li, Shao-Lun Huang, Lin Zhang, Lizhong Zheng, Amir Zamir, and Leonidas Guibas. An information-theoretic approach to transferability in task transfer learning. In *2019 IEEE international conference on image processing (ICIP)*, pages 2309–2313. IEEE, 2019.
- [4] Daniel Bolya, Rohit Mittapalli, and Judy Hoffman. Scalable diverse model selection for accessible transfer learning. In Marc’Aurelio Ranzato, Alina Beygelzimer, Yann N. Dauphin, Percy Liang, and Jennifer Wortman Vaughan, editors, *Advances in Neural Information Processing Systems 34: Annual Conference on Neural Information Processing Systems 2021, NeurIPS 2021, December 6-14, 2021, virtual*, pages 19301–19312, 2021. URL <https://proceedings.neurips.cc/paper/2021/hash/a1140a3d0df1c81e24ae954d935e8926-Abstract.html>.
- [5] Han Cai, Chuang Gan, and Song Han. Efficientvit: Enhanced linear attention for high-resolution low-computation visual recognition. *arXiv preprint arXiv:2205.14756*, 2022.
- [6] Mathilde Caron, Hugo Touvron, Ishan Misra, Hervé Jégou, Julien Mairal, Piotr Bojanowski, and Armand Joulin. Emerging properties in self-supervised vision transformers. In *Proceedings of the IEEE/CVF international conference on computer vision*, pages 9650–9660, 2021.
- [7] Chengpeng Chen, Zichao Guo, Haien Zeng, Pengfei Xiong, and Jian Dong. Repghost: A hardware-efficient ghost module via re-parameterization. *arXiv preprint arXiv:2211.06088*, 2022.
- [8] Ting Chen, Simon Kornblith, Mohammad Norouzi, and Geoffrey Hinton. A simple framework for contrastive learning of visual representations. In *International conference on machine learning*, pages 1597–1607. PMLR, 2020.
- [9] Xiangning Chen, Cho-Jui Hsieh, and Boqing Gong. When vision transformers outperform resnets without pre-training or strong data augmentations. *arXiv preprint arXiv:2106.01548*, 2021.
- [10] Xinlei Chen, Zhuang Liu, Saining Xie, and Kaiming He. Deconstructing denoising diffusion models for self-supervised learning. *arXiv preprint arXiv:2401.14404*, 2024.
- [11] Mehdi Cherti, Romain Beaumont, Ross Wightman, Mitchell Wortsman, Gabriel Ilharco, Cade Gordon, Christoph Schuhmann, Ludwig Schmidt, and Jenia Jitsev. Reproducible scaling laws for contrastive language-image learning. In *Proceedings of the IEEE/CVF Conference on Computer Vision and Pattern Recognition*, pages 2818–2829, 2023.

- [12] Adam Coates, Andrew Ng, and Honglak Lee. An analysis of single-layer networks in unsupervised feature learning. In *Proceedings of the fourteenth international conference on artificial intelligence and statistics*, pages 215–223. JMLR Workshop and Conference Proceedings, 2011.
- [13] Zihang Dai, Hanxiao Liu, Quoc V Le, and Mingxing Tan. Coatnet: Marrying convolution and attention for all data sizes. *Advances in neural information processing systems*, 34:3965–3977, 2021.
- [14] Alexey Dosovitskiy, Lucas Beyer, Alexander Kolesnikov, Dirk Weissenborn, Xiaohua Zhai, Thomas Unterthiner, Mostafa Dehghani, Matthias Minderer, Georg Heigold, Sylvain Gelly, Jakob Uszkoreit, and Neil Houlsby. An image is worth 16x16 words: Transformers for image recognition at scale. *CoRR*, abs/2010.11929, 2020. URL <https://arxiv.org/abs/2010.11929>.
- [15] Kai Han, Yunhe Wang, Qi Tian, Jianyuan Guo, Chunjing Xu, and Chang Xu. Ghostnet: More features from cheap operations. In *Proceedings of the IEEE/CVF conference on computer vision and pattern recognition*, pages 1580–1589, 2020.
- [16] Kaiming He, Xiangyu Zhang, Shaoqing Ren, and Jian Sun. Deep residual learning for image recognition. *CoRR*, abs/1512.03385, 2015. URL <http://arxiv.org/abs/1512.03385>.
- [17] Kaiming He, Xinlei Chen, Saining Xie, Yanghao Li, Piotr Dollár, and Ross Girshick. Masked autoencoders are scalable vision learners. In *Proceedings of the IEEE/CVF conference on computer vision and pattern recognition*, pages 16000–16009, 2022.
- [18] Tong He, Zhi Zhang, Hang Zhang, Zhongyue Zhang, Junyuan Xie, and Mu Li. Bag of tricks for image classification with convolutional neural networks. In *Proceedings of the IEEE/CVF conference on computer vision and pattern recognition*, pages 558–567, 2019.
- [19] Andrew Howard, Mark Sandler, Grace Chu, Liang-Chieh Chen, Bo Chen, Mingxing Tan, Weijun Wang, Yukun Zhu, Ruoming Pang, Vijay Vasudevan, et al. Searching for mobilenetv3. In *Proceedings of the IEEE/CVF international conference on computer vision*, pages 1314–1324, 2019.
- [20] Jie Hu, Li Shen, and Gang Sun. Squeeze-and-excitation networks. In *Proceedings of the IEEE conference on computer vision and pattern recognition*, pages 7132–7141, 2018.
- [21] Tianyu Hua, Wenxiao Wang, Zihui Xue, Sucheng Ren, Yue Wang, and Hang Zhao. On feature decorrelation in self-supervised learning. In *Proceedings of the IEEE/CVF International Conference on Computer Vision (ICCV)*, pages 9598–9608, October 2021.
- [22] Gao Huang, Zhuang Liu, Laurens Van Der Maaten, and Kilian Q Weinberger. Densely connected convolutional networks. In *Proceedings of the IEEE conference on computer vision and pattern recognition*, pages 4700–4708, 2017.
- [23] Long-Kai Huang, Junzhou Huang, Yu Rong, Qiang Yang, and Ying Wei. Frustratingly easy transferability estimation. In Kamalika Chaudhuri, Stefanie Jegelka, Le Song, Csaba Szepesvári, Gang Niu, and Sivan Sabato, editors, *International Conference on Machine Learning, ICML 2022, 17-23 July 2022, Baltimore, Maryland, USA*, volume 162 of *Proceedings of Machine Learning Research*, pages 9201–9225. PMLR, 2022. URL <https://proceedings.mlr.press/v162/huang22d.html>.
- [24] George Klir and Bo Yuan. *Fuzzy sets and fuzzy logic*, volume 4. Prentice hall New Jersey, 1995.
- [25] Alex Krizhevsky, Geoffrey Hinton, et al. Learning multiple layers of features from tiny images. 2009.
- [26] Alex Krizhevsky, Ilya Sutskever, and Geoffrey E Hinton. Imagenet classification with deep convolutional neural networks. In F. Pereira, C.J. Burges, L. Bottou, and K.Q. Weinberger, editors, *Advances in Neural Information Processing Systems*, volume 25. Curran Associates, Inc., 2012. URL https://proceedings.neurips.cc/paper_files/paper/2012/file/c399862d3b9d6b76c8436e924a68c45b-Paper.pdf.
- [27] Xinran Liu, Yikun Bai, Yuzhe Lu, Andrea Soltoggio, and Soheil Kolouri. Wasserstein task embedding for measuring task similarities, 2022.
- [28] Xinyu Liu, Houwen Peng, Ningxin Zheng, Yuqing Yang, Han Hu, and Yixuan Yuan. Efficientvit: Memory efficient vision transformer with cascaded group attention. In *Proceedings of the IEEE/CVF Conference on Computer Vision and Pattern Recognition*, pages 14420–14430, 2023.

- [29] Ze Liu, Yutong Lin, Yue Cao, Han Hu, Yixuan Wei, Zheng Zhang, Stephen Lin, and Baining Guo. Swin transformer: Hierarchical vision transformer using shifted windows. In *Proceedings of the IEEE/CVF international conference on computer vision*, pages 10012–10022, 2021.
- [30] Ze Liu, Han Hu, Yutong Lin, Zhuliang Yao, Zhenda Xie, Yixuan Wei, Jia Ning, Yue Cao, Zheng Zhang, Li Dong, Furu Wei, and Baining Guo. Swin transformer V2: scaling up capacity and resolution. In *IEEE/CVF Conference on Computer Vision and Pattern Recognition, CVPR 2022, New Orleans, LA, USA, June 18-24, 2022*, pages 11999–12009. IEEE, 2022. doi: 10.1109/CVPR52688.2022.01170. URL <https://doi.org/10.1109/CVPR52688.2022.01170>.
- [31] Zhuang Liu, Hanzi Mao, Chao-Yuan Wu, Christoph Feichtenhofer, Trevor Darrell, and Saining Xie. A convnet for the 2020s. In *Proceedings of the IEEE/CVF conference on computer vision and pattern recognition*, pages 11976–11986, 2022.
- [32] Ningning Ma, Xiangyu Zhang, Hai-Tao Zheng, and Jian Sun. Shufflenet V2: practical guidelines for efficient CNN architecture design. In Vittorio Ferrari, Martial Hebert, Cristian Sminchisescu, and Yair Weiss, editors, *Computer Vision - ECCV 2018 - 15th European Conference, Munich, Germany, September 8-14, 2018, Proceedings, Part XIV*, volume 11218 of *Lecture Notes in Computer Science*, pages 122–138. Springer, 2018. doi: 10.1007/978-3-030-01264-9_8. URL https://doi.org/10.1007/978-3-030-01264-9_8.
- [33] Cuong Nguyen, Tal Hassner, Matthias Seeger, and Cedric Archambeau. Leep: A new measure to evaluate transferability of learned representations. In *International Conference on Machine Learning*, pages 7294–7305. PMLR, 2020.
- [34] Michal Pándy, Andrea Agostinelli, Jasper R. R. Uijlings, Vittorio Ferrari, and Thomas Mensink. Transferability estimation using bhattacharyya class separability. In *IEEE/CVF Conference on Computer Vision and Pattern Recognition, CVPR 2022, New Orleans, LA, USA, June 18-24, 2022*, pages 9162–9172. IEEE, 2022. doi: 10.1109/CVPR52688.2022.00896. URL <https://doi.org/10.1109/CVPR52688.2022.00896>.
- [35] Alec Radford, Jong Wook Kim, Chris Hallacy, Aditya Ramesh, Gabriel Goh, Sandhini Agarwal, Girish Sastry, Amanda Askell, Pamela Mishkin, Jack Clark, et al. Learning transferable visual models from natural language supervision. In *International conference on machine learning*, pages 8748–8763. PMLR, 2021.
- [36] Ilija Radosavovic, Raj Prateek Kosaraju, Ross Girshick, Kaiming He, and Piotr Dollár. Designing network design spaces. In *Proceedings of the IEEE/CVF conference on computer vision and pattern recognition*, pages 10428–10436, 2020.
- [37] Mark Sandler, Andrew Howard, Menglong Zhu, Andrey Zhmoginov, and Liang-Chieh Chen. Mobilenetv2: Inverted residuals and linear bottlenecks. In *Proceedings of the IEEE conference on computer vision and pattern recognition*, pages 4510–4520, 2018.
- [38] Andreas Steiner, Alexander Kolesnikov, Xiaohua Zhai, Ross Wightman, Jakob Uszkoreit, and Lucas Beyer. How to train your vit? data, augmentation, and regularization in vision transformers. *arXiv preprint arXiv:2106.10270*, 2021.
- [39] Christian Szegedy, Wei Liu, Yangqing Jia, Pierre Sermanet, Scott Reed, Dragomir Anguelov, Dumitru Erhan, Vincent Vanhoucke, and Andrew Rabinovich. Going deeper with convolutions. In *Proceedings of the IEEE conference on computer vision and pattern recognition*, pages 1–9, 2015.
- [40] Christian Szegedy, Vincent Vanhoucke, Sergey Ioffe, Jon Shlens, and Zbigniew Wojna. Rethinking the inception architecture for computer vision. In *Proceedings of the IEEE conference on computer vision and pattern recognition*, pages 2818–2826, 2016.
- [41] Mingxing Tan and Quoc Le. Efficientnet: Rethinking model scaling for convolutional neural networks. In *International conference on machine learning*, pages 6105–6114. PMLR, 2019.
- [42] Mingxing Tan and Quoc Le. Efficientnetv2: Smaller models and faster training. In *International conference on machine learning*, pages 10096–10106. PMLR, 2021.
- [43] Mingxing Tan, Bo Chen, Ruoming Pang, Vijay Vasudevan, Mark Sandler, Andrew Howard, and Quoc V. Le. Mnasnet: Platform-aware neural architecture search for mobile. In *Proceedings of the IEEE/CVF Conference on Computer Vision and Pattern Recognition (CVPR)*, June 2019.
- [44] Yehui Tang, Kai Han, Jianyuan Guo, Chang Xu, Chao Xu, and Yunhe Wang. Ghostnetv2: enhance cheap operation with long-range attention. *Advances in Neural Information Processing Systems*, 35:9969–9982, 2022.

- [45] Zhengzhong Tu, Hossein Talebi, Han Zhang, Feng Yang, Peyman Milanfar, Alan Bovik, and Yinxiao Li. Maxvit: Multi-axis vision transformer. In *European conference on computer vision*, pages 459–479. Springer, 2022.
- [46] Pavan Kumar Anasosalu Vasu, James Gabriel, Jeff Zhu, Oncel Tuzel, and Anurag Ranjan. Mobileone: An improved one millisecond mobile backbone. In *Proceedings of the IEEE/CVF Conference on Computer Vision and Pattern Recognition*, pages 7907–7917, 2023.
- [47] Jingdong Wang, Ke Sun, Tianheng Cheng, Borui Jiang, Chaorui Deng, Yang Zhao, Dong Liu, Yadong Mu, Mingkui Tan, Xinggang Wang, et al. Deep high-resolution representation learning for visual recognition. *IEEE transactions on pattern analysis and machine intelligence*, 43(10): 3349–3364, 2020.
- [48] Liwei Wang, Lunjia Hu, Jiayuan Gu, Zhiqiang Hu, Yue Wu, Kun He, and John Hopcroft. Towards understanding learning representations: To what extent do different neural networks learn the same representation. *Advances in neural information processing systems*, 31, 2018.
- [49] Wenxiao Wang and Soheil Feizi. Temporal robustness against data poisoning. *CoRR*, abs/2302.03684, 2023. doi: 10.48550/ARXIV.2302.03684. URL <https://doi.org/10.48550/arXiv.2302.03684>.
- [50] Saining Xie, Ross Girshick, Piotr Dollár, Zhuowen Tu, and Kaiming He. Aggregated residual transformations for deep neural networks. In *Proceedings of the IEEE conference on computer vision and pattern recognition*, pages 1492–1500, 2017.
- [51] Kaichao You, Yong Liu, Mingsheng Long, and Jianmin Wang. Logme: Practical assessment of pre-trained models for transfer learning. *CoRR*, abs/2102.11005, 2021. URL <https://arxiv.org/abs/2102.11005>.
- [52] Weihao Yu, Pan Zhou, Shuicheng Yan, and Xinchao Wang. Inceptionnext: When inception meets convnext. *arXiv preprint arXiv:2303.16900*, 2023.
- [53] Lotfi A Zadeh. Fuzzy sets. *Information and control*, 8(3):338–353, 1965.
- [54] Sergey Zagoruyko and Nikos Komodakis. Wide residual networks. *CoRR*, abs/1605.07146, 2016. URL <http://arxiv.org/abs/1605.07146>.
- [55] Amir R Zamir, Alexander Sax, William Shen, Leonidas J Guibas, Jitendra Malik, and Silvio Savarese. Taskonomy: Disentangling task transfer learning. In *Proceedings of the IEEE conference on computer vision and pattern recognition*, pages 3712–3722, 2018.
- [56] Wangchunshu Zhou, Canwen Xu, and Julian J. McAuley. Efficiently tuned parameters are task embeddings. In Yoav Goldberg, Zornitsa Kozareva, and Yue Zhang, editors, *Proceedings of the 2022 Conference on Empirical Methods in Natural Language Processing, EMNLP 2022, Abu Dhabi, United Arab Emirates, December 7-11, 2022*, pages 5007–5014. Association for Computational Linguistics, 2022. doi: 10.18653/v1/2022.emnlp-main.334. URL <https://doi.org/10.18653/v1/2022.emnlp-main.334>.

A Full List of Candidate Models Used in The Experiments

Table 3: A full list of the 100 pre-trained models that are used as the candidate models in the experiments.

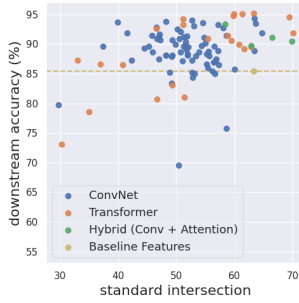
index	name (used by the corresponding source)	category	source	index	name (used by the corresponding source)	category	source
1	ResNet18_Weights.IMAGENET1K_V1	ConvNet	torchvision	51	ShuffleNet_V2_X1_0_Weights.IMAGENET1K_V1	ConvNet	torchvision
2	EfficientNet_B0_Weights.IMAGENET1K_V1	ConvNet	torchvision	52	ShuffleNet_V2_X1_5_Weights.IMAGENET1K_V1	ConvNet	torchvision
3	GoogLeNet_Weights.IMAGENET1K_V1	ConvNet	torchvision	53	ShuffleNet_V2_X2_0_Weights.IMAGENET1K_V1	ConvNet	torchvision
4	Swin_T_Weights.IMAGENET1K_V1	Transformer	torchvision	54	Swin_V2_T_Weights.IMAGENET1K_V1	Transformer	torchvision
5	MobileNet_V3_Large_Weights.IMAGENET1K_V1	ConvNet	torchvision	55	ViT_B_32_Weights.IMAGENET1K_V1	Transformer	torchvision
6	MobileNet_V3_Large_Weights.IMAGENET1K_V2	ConvNet	torchvision	56	ViT_B_16_Weights.IMAGENET1K_V1	Transformer	torchvision
7	MobileNet_V3_Small_Weights.IMAGENET1K_V1	ConvNet	torchvision	57	ViT_B_16_Weights.IMAGENET1K_SWAG_LINEAR_V1	Transformer	torchvision
8	MNASNet0_5_Weights.IMAGENET1K_V1	ConvNet	torchvision	58	Wide_ResNet50_2_Weights.IMAGENET1K_V1	ConvNet	torchvision
9	ShuffleNet_V2_X0_5_Weights.IMAGENET1K_V1	ConvNet	torchvision	59	Wide_ResNet50_2_Weights.IMAGENET1K_V2	ConvNet	torchvision
10	AlexNet_Weights.IMAGENET1K_V1	ConvNet	torchvision	60	mobileone_s0	ConvNet	timm
11	ConvNeXt_Tiny_Weights.IMAGENET1K_V1	ConvNet	torchvision	61	mobileone_s1	ConvNet	timm
12	ConvNeXt_Small_Weights.IMAGENET1K_V1	ConvNet	torchvision	62	mobileone_s2	ConvNet	timm
13	DenseNet121_Weights.IMAGENET1K_V1	ConvNet	torchvision	63	mobileone_s3	ConvNet	timm
14	DenseNet161_Weights.IMAGENET1K_V1	ConvNet	torchvision	64	mobileone_s4	ConvNet	timm
15	DenseNet169_Weights.IMAGENET1K_V1	ConvNet	torchvision	65	inception_next_tiny.sail_in1k	ConvNet	timm
16	DenseNet201_Weights.IMAGENET1K_V1	ConvNet	torchvision	66	inception_next_small.sail_in1k	ConvNet	timm
17	EfficientNet_B1_Weights.IMAGENET1K_V1	ConvNet	torchvision	67	inception_next_base.sail_in1k	ConvNet	timm
18	EfficientNet_B2_Weights.IMAGENET1K_V1	ConvNet	torchvision	68	ghostnet_100.in1k	ConvNet	timm
19	EfficientNet_B3_Weights.IMAGENET1K_V1	ConvNet	torchvision	69	ghostnetv2_100.in1k	ConvNet	timm
20	EfficientNet_B4_Weights.IMAGENET1K_V1	ConvNet	torchvision	70	ghostnetv2_130.in1k	ConvNet	timm
21	EfficientNet_V2_S_Weights.IMAGENET1K_V1	ConvNet	torchvision	71	ghostnetv2_160.in1k	ConvNet	timm
22	Inception_V3_Weights.IMAGENET1K_V1	ConvNet	torchvision	72	reghostnet_050.in1k	ConvNet	timm
23	MNASNet0_75_Weights.IMAGENET1K_V1	ConvNet	torchvision	73	reghostnet_058.in1k	ConvNet	timm
24	MNASNet1_0_Weights.IMAGENET1K_V1	ConvNet	torchvision	74	reghostnet_080.in1k	ConvNet	timm
25	MNASNet1_3_Weights.IMAGENET1K_V1	ConvNet	torchvision	75	reghostnet_100.in1k	ConvNet	timm
26	MobileNet_V2_Weights.IMAGENET1K_V1	ConvNet	torchvision	76	efficientvit_b0.r224_in1k	Transformer	timm
27	MobileNet_V2_Weights.IMAGENET1K_V2	ConvNet	torchvision	77	efficientvit_b1.r224_in1k	Transformer	timm
28	RegNet_X_1_6GF_Weights.IMAGENET1K_V1	ConvNet	torchvision	78	efficientvit_b2.r224_in1k	Transformer	timm
29	RegNet_X_1_6GF_Weights.IMAGENET1K_V2	ConvNet	torchvision	79	efficientvit_b3.r224_in1k	Transformer	timm
30	RegNet_X_3_2GF_Weights.IMAGENET1K_V1	ConvNet	torchvision	80	efficientvit_m0.r224_in1k	Transformer	timm
31	RegNet_X_3_2GF_Weights.IMAGENET1K_V2	ConvNet	torchvision	81	efficientvit_m1.r224_in1k	Transformer	timm
32	RegNet_X_400MF_Weights.IMAGENET1K_V1	ConvNet	torchvision	82	efficientvit_m2.r224_in1k	Transformer	timm
33	RegNet_X_400MF_Weights.IMAGENET1K_V2	ConvNet	torchvision	83	efficientvit_m3.r224_in1k	Transformer	timm
34	RegNet_X_800MF_Weights.IMAGENET1K_V1	ConvNet	torchvision	84	efficientvit_m4.r224_in1k	Transformer	timm
35	RegNet_X_800MF_Weights.IMAGENET1K_V2	ConvNet	torchvision	85	efficientvit_m5.r224_in1k	Transformer	timm
36	RegNet_Y_1_6GF_Weights.IMAGENET1K_V1	ConvNet	torchvision	86	coatnet_nano_rw_224.sw_in1k	Hybrid (Conv + Attention)	timm
37	RegNet_Y_1_6GF_Weights.IMAGENET1K_V2	ConvNet	torchvision	87	coatnext_nano_rw_224.sw_in1k	Hybrid (Conv + Attention)	timm
38	RegNet_Y_3_2GF_Weights.IMAGENET1K_V1	ConvNet	torchvision	88	seresnext101_32x4d_gluon_in1k	ConvNet	timm
39	RegNet_Y_3_2GF_Weights.IMAGENET1K_V2	ConvNet	torchvision	89	vit_tiny_r_s16_p8_224.augreg_in21k	Transformer	timm
40	RegNet_Y_400MF_Weights.IMAGENET1K_V1	ConvNet	torchvision	90	vit_small_r26_s32_224.augreg_in21k	Transformer	timm
41	RegNet_Y_400MF_Weights.IMAGENET1K_V2	ConvNet	torchvision	91	vit_tiny_r_s16_p8_224.augreg_in21k_ft_in1k	Transformer	timm
42	RegNet_Y_800MF_Weights.IMAGENET1K_V1	ConvNet	torchvision	92	vit_small_r26_s32_224.augreg_in21k_ft_in1k	Transformer	timm
43	RegNet_Y_800MF_Weights.IMAGENET1K_V2	ConvNet	torchvision	93	hnnet_w18_small_gluon_in1k	ConvNet	timm
44	ResNeXt0_32X4D_Weights.IMAGENET1K_V1	ConvNet	torchvision	94	hnnet_w18_small_v2_gluon_in1k	ConvNet	timm
45	ResNeXt0_32X4D_Weights.IMAGENET1K_V2	ConvNet	torchvision	95	vit_small_patch16_224.dino	Transformer	timm
46	ResNet101_Weights.IMAGENET1K_V1	ConvNet	torchvision	96	vit_base_patch16_224.mae	Transformer	timm
47	ResNet101_Weights.IMAGENET1K_V2	ConvNet	torchvision	97	maxvit_tiny_rw_224.in1k	Hybrid (Conv + Attention)	timm
48	ResNet50_Weights.IMAGENET1K_V1	ConvNet	torchvision	98	maxvit_tiny_rw_224.sw_in1k	Hybrid (Conv + Attention)	timm
49	ResNet50_Weights.IMAGENET1K_V2	ConvNet	torchvision	99	vit_base_patch32_224.sam_in1k	Transformer	timm
50	ResNet34_Weights.IMAGENET1K_V1	ConvNet	torchvision	100	vit_base_patch32_clip_224.openai_ft_in1k	Transformer	timm

In Table 3, we include the full list of pre-trained models that are used in our evaluations. We include as follows relevant references and corresponding model indices in Table 3 (note that some pre-trained models correspond to multiple references):

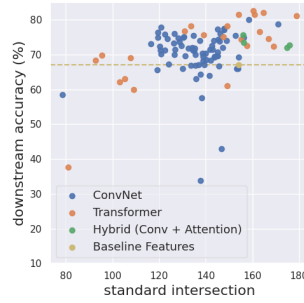
- ResNet [16]: 1, 46, 47, 48, 49, 50, 88;
- EfficientNet/EfficientNetV2 [41, 42]: 2, 17, 18, 19, 20, 21;
- GoogLeNet [39]: 3;
- Swin Transformer/Swin Transformer V2 [29, 30]: 4, 54;
- MobileNet V2/V3 [37, 19]: 5, 6, 7, 26, 27;
- MNASNet [43]: 8, 23, 24, 25;
- ShuffleNet V2 [32]: 9, 51, 52, 53;
- AlexNet [26]: 10;
- ConvNeXt [31]: 11, 12, 87;
- DenseNet [22]: 13, 14, 15, 16;
- Inception V3 [40]: 22;
- RegNet [36]: 28, 29, 30, 31, 32, 33, 34, 35, 36, 37, 38, 39, 40, 41, 42, 43;
- ResNeXt [50]: 44, 45, 88;
- Vision Transformer [14]: 55, 56, 57, 89, 90, 91, 92, 95, 96, 99, 100;
- Wide ResNet [54]: 58, 59;
- MobileOne [46]: 60, 61, 62, 63, 64;
- InceptionNeXt [52]: 65, 66, 67;
- GhostNet/GhostNetV2 [15, 44]: 68, 69, 70, 71;

- RepGhostNet [7]: 72, 73, 74, 75;
- EfficientViT (MIT) [5]: 76, 77, 78, 79;
- EfficientViT (MSRA) [28]: 80, 81, 82, 83, 84, 85;
- CoAtNet [13]: 86, 87;
- Squeeze-and-Excitation [20]: 88;
- Bag-of-Tricks [18]: 88;
- AugReg [38]: 89, 90, 91, 92;
- HRNet [47]: 93, 94;
- DINO [6]: 95;
- Masked Autoencoder [17]: 96;
- MaxViT [45]: 97, 98;
- Sharpness-aware minimizer for ViT [9]: 99;
- Reproducible scaling laws [11]: 100;
- CLIP [35]: 100.

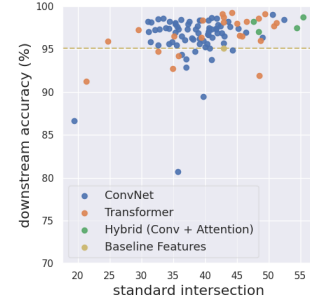
B Figures of Empirical Evaluations



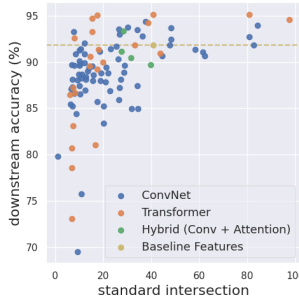
(a) downstream: CIFAR-10
baseline features: ResNet-18



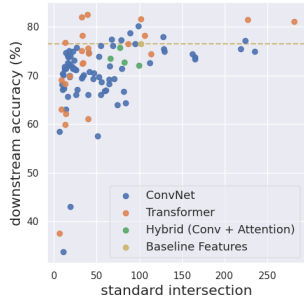
(b) downstream: CIFAR-100
baseline features: ResNet-18



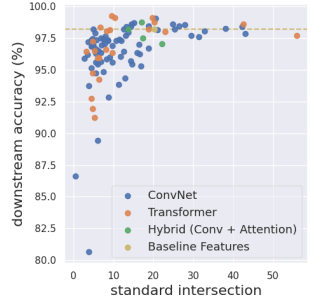
(c) downstream: STL-10
baseline features: ResNet-18



(d) downstream: CIFAR-10
baseline features: Swin-T (tiny)

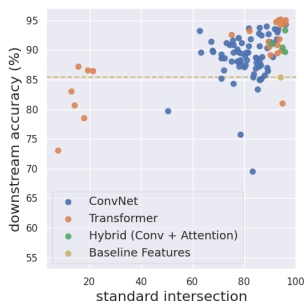


(e) downstream: CIFAR-100
baseline features: Swin-T (tiny)

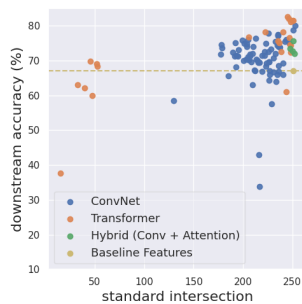


(f) downstream: STL-10
baseline features: Swin-T (tiny)

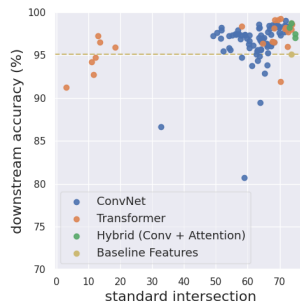
Figure 4: Downstream accuracy (i.e. the ground truth) v.s. the cardinality of standard intersections (i.e. the selection metric) when using 4k steps per candidate. The downstream accuracy of the baseline features are highlighted with the dashed line. When a public model is only suboptimal, using it as baseline features for Standardized Embedder can still locate more competitive models.



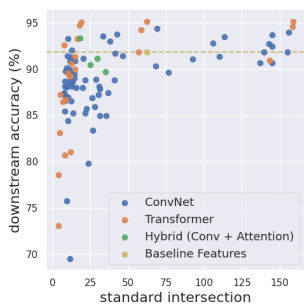
(a) downstream: CIFAR-10
baseline features: ResNet-18



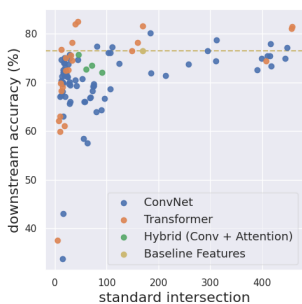
(b) downstream: CIFAR-100
baseline features: ResNet-18



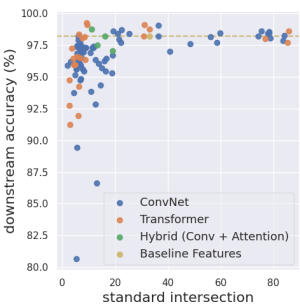
(c) downstream: STL-10
baseline features: ResNet-18



(d) downstream: CIFAR-10
baseline features: Swin-T (tiny)



(e) downstream: CIFAR-100
baseline features: Swin-T (tiny)



(f) downstream: STL-10
baseline features: Swin-T (tiny)

Figure 5: Downstream accuracy (i.e. the ground truth) v.s. the cardinality of standard intersections (i.e. the selection metric) when using 10k steps per candidate. The downstream accuracy of the baseline features are highlighted with the dashed line. When a public model is only suboptimal, using it as baseline features for Standardized Embedder can still locate more competitive models.

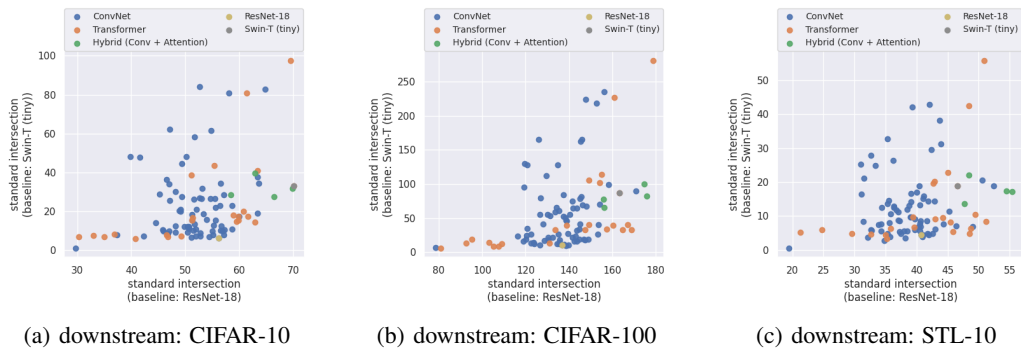


Figure 6: Comparing the cardinality of standard intersections (i.e. the selection metric) when using different baseline features (ResNet-18 and Swin-T (tiny)) with 4k steps per candidate. The green/orange points in the bottom right suggest using ResNet-18 as baseline features tend to overestimate (some) models with attentions compared to using Swin Transformer (tiny).

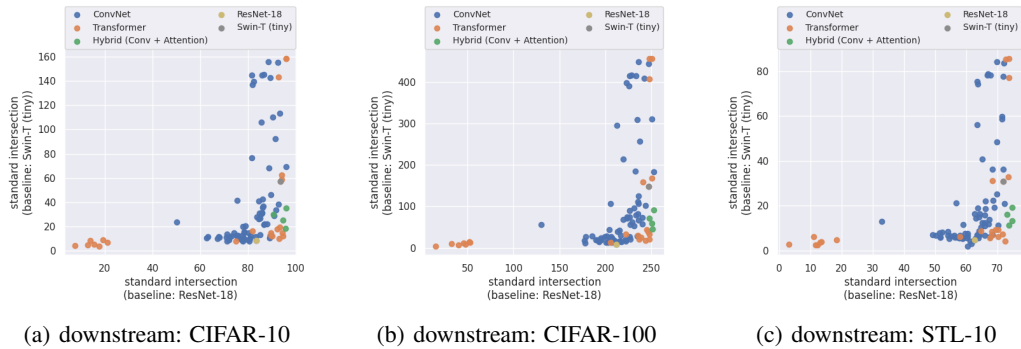
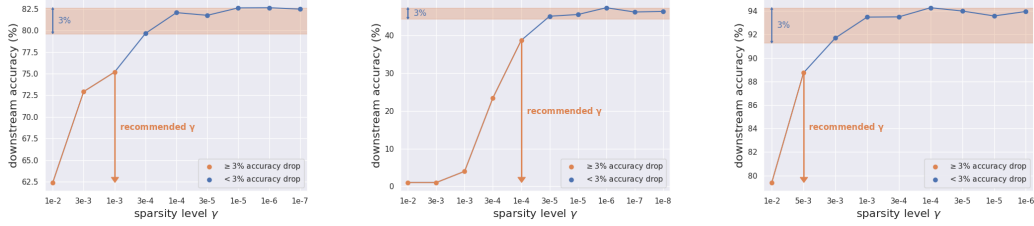


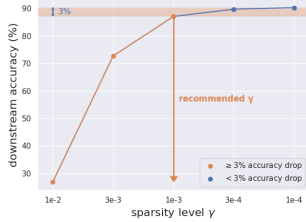
Figure 7: Comparing the cardinality of standard intersections (i.e. the selection metric) when using different baseline features (ResNet-18 and Swin-T (tiny)) with 10k steps per candidate. The green/orange points in the bottom right suggest using ResNet-18 as baseline features tend to overestimate (some) models with attentions compared to using Swin Transformer (tiny).



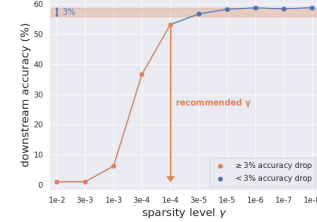
(a) downstream: CIFAR-10
baseline features: ResNet-18

(b) downstream: CIFAR-100
baseline features: ResNet-18

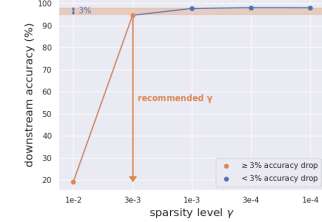
(c) downstream: STL-10
baseline features: ResNet-18



(d) downstream: CIFAR-10
baseline features: Swin-T (tiny)



(e) downstream: CIFAR-100
baseline features: Swin-T (tiny)



(f) downstream: STL-10
baseline features: Swin-T (tiny)

Figure 8: Downstream accuracy of the baseline features corresponding to varying level of sparsity regularization γ . A rule of thumb for deciding the value of γ : using the smallest γ with at least 3% accuracy drop from the converged accuracy.

C Illustrative Example for Section 4.2

Here is an example to illustrate how to associate every subset of the baseline feature set B with a binary vector from $\{0, 1\}^N$. Assuming now the baseline feature set $B : \mathcal{X} \rightarrow \mathbb{R}^N$ contains a total of $N = 4$ features, b_0, b_1, b_2, b_3 , where each of them is a function from \mathcal{X} to \mathbb{R} , then there will be a total of $2^4 = 16$ different subsets of B . We can associate each subset with a distinct, 4-dimensional binary vector (i.e. a vector in $\{0, 1\}^4$) by using 1 to indicate the presence of a feature and 0 to indicate an absence of a feature in the subset. Specifically, $(0, 0, 0, 0)$ will denote the empty subset, $(0, 0, 1, 0)$ will denote $\{b_2\}$ and $(1, 0, 1, 1)$ will denote $\{b_0, b_2, b_3\}$.

D Broader Impacts

When selecting models locally, asymptotically fast update and selection indicate considerably improved scalability, which is obviously positive as one can potentially utilize more candidate models. Meanwhile, the decentralizability of isolated model embedding naturally relates to a potential application: a decentralized model market with a decentralized model selection system.

There are, of course, positive impacts from having such a decentralized model market. For individual downstream users, their capabilities can be extended by effectively accessing more candidate models, and their costs for model selection can be potentially reduced through systematic and out-of-the-box selection operations. For model owners, their profits can be enlarged by promoting their models to more potential users.

However, while the benefits of such a decentralized market stem from the accelerated distribution of models, the distribution of malicious behaviors, such as backdoors, may also be facilitated in the presence of hostile parties, which is potentially a negative impact and a new research direction.